Indirect study of low-energy resonances in $^{31}P(p,\alpha)^{28}Si$ and $^{35}Cl(p,\alpha)^{32}S$

J. G. Ross,* J. Görres, C. Iliadis,† S. Vouzoukas, and M. Wiescher
Department of Physics, University of Notre Dame, Notre Dame, Indiana 46556

R. B. Vogelaar
Department of Physics, Princeton University, Princeton, New Jersey 08544

S. Utku,‡ N. P. T. Bateman, and P. D. Parker
A. W. Wright Nuclear Structure Laboratory, Yale University, New Haven, Connecticut 06511
(Received 9 May 1995)

The reaction sequences governing the reaction flow in the *rp* process are important for the understanding of the energy generation and nucleosynthesis of heavy elements in hot and explosive stellar hydrogen burning. Of considerable interest are (p,α) reactions along the process path which lead to the formation of reaction cycles rather than to chains of proton capture processes and β decays. Previous direct attempts to measure the low-energy reaction cross sections for $^{31}P(p,\alpha)^{28}Si$ and $^{35}Cl(p,\alpha)^{32}S$ resulted only in upper limits for the strengths of possible low-energy resonances which may dominate the reaction rates. In this paper an indirect experimental approach is presented to study the structure of the low-energy unbound states in the compound nuclei ^{32}S and ^{36}Ar. The results allow a more accurate determination of the contributions of these low-energy levels in the (p,α) reaction channel.

PACS number(s): 25.40.Ny, 25.40.Hs, 27.30.+t, 97.10.Cv

I. INTRODUCTION

The nuclear processes and reaction sequences in stellar and explosive hydrogen burning scenarios determine the time scales, energy generation, and nucleosynthesis at different temperature and density conditions [1,2]. In various astrophysical sites, hydrogen burning may take place via two kinds of possible reaction sequences. In the first of these, chains of (p,γ) reactions and β decays fuse the initial material towards heavier masses; this characterizes the *pp* chains and the *rp* process [1]. There are many cases, however, where the reaction flow is not serial but cyclic.

Cycling can occur if the α threshold is lower than the proton threshold in the compound nucleus formed by a proton capture reaction. This is mainly the case for $T=0$ nuclei close to the line of stability and therefore occurs predominantly at lower stellar temperature conditions, $T \leq 0.4$ GK. Cyclic reaction sequences of (p,γ) reactions and β decays are then closed by a (p,α) reaction, as in the CNO cycles, and the initial catalytic material is stored in the cycle for a certain amount of time $\tau_{\rm cycl}$. This causes a temporary enrichment of the abundances of the isotopes within the cycle which can only be depleted by breakout or leakage reactions.

The dominant leakage reaction at lower temperature conditions is the (p,γ) reaction on the $T=1/2$ nucleus which competes with the (p,α) reaction. These reaction branchings determine the time period $\tau_{\rm cycl}$, given by

$$\tau_{\rm cycl}=\left(\frac{\langle\sigma v\rangle_{(p,\gamma)}+\langle\sigma v\rangle_{(p,\alpha)}}{\langle\sigma v\rangle_{(p,\gamma)}}\right)\left[\sum_j \tau_j^c\right], \qquad (1)$$

where τ_j^c are the lifetimes of the isotopes in the reaction cycle and $\langle\sigma v\rangle_{(p,\gamma)}$, $\langle\sigma v\rangle_{(p,\alpha)}$ are the reaction rates for the (p,γ) and (p,α) reactions, respectively. Large break-out rates limit the storage time to the sum of the lifetimes of the isotopes in the cycle. For small leakage rates the storage time becomes large, eventually larger than the macroscopic time scale of the astrophysical scenario. In the case of the *rp* process, the cycle is then the end point of the nucleosynthesis, and the equilibrium abundance distribution in the cycle will be reflected in the final nucleosynthesis abundance distribution [2]. Figure 1 shows the various possible reaction cycles (CNO, NeNa, SiP, and SCl) at conditions of hot hydrogen burning, in this example at the peak temperatures of novae events, $T \approx 0.2$–0.4 GK [3,4]. Therefore, to understand the influence of reaction cycles for the nucleosynthesis of heavy elements in the *rp* process it is important to study the (p,α) reactions on $T=1/2$ nuclei like ^{23}Na, ^{27}Al, ^{31}P, and ^{35}Cl, as well as the competing (p,γ) reactions on these isotopes to determine the reaction branchings.

Several attempts have been made in recent years to directly measure the low-energy resonances in the $^{23}Na(p,\gamma),(p,\alpha)$ [5], the $^{27}Al(p,\gamma),(p,\alpha)$ [6], the $^{31}P(p,\gamma),(p,\alpha)$ [7,8], and the $^{35}Cl(p,\gamma),(p,\alpha)$ [9] reactions. The previous studies of proton capture reactions on ^{23}Na indicate that the NeNa cycle is closed at temperatures $T_9 \leq 0.2$, but the studies of proton capture on ^{27}Al clearly indicate that the cycle is open even at low temperatures because of the strong $^{27}Al(p,\gamma)^{28}Si$ reaction [6,10,11].

In the case of the SiP and SCl cycles, however, the situation is unclear. The $^{31}P(p,\gamma)^{32}S$ and $^{35}Cl(p,\gamma)^{36}Ar$ reactions are characterized by many resonances in the energy

*Present address: Department of Physics and Astronomy, University of Central Arkansas, Conway, AR 70235.
†Present address: TRIUMF, Vancouver, B.C. V6T 2A3, Canada.
‡Present address: Columbia University, H905F East Campus, New York, NY 10027.

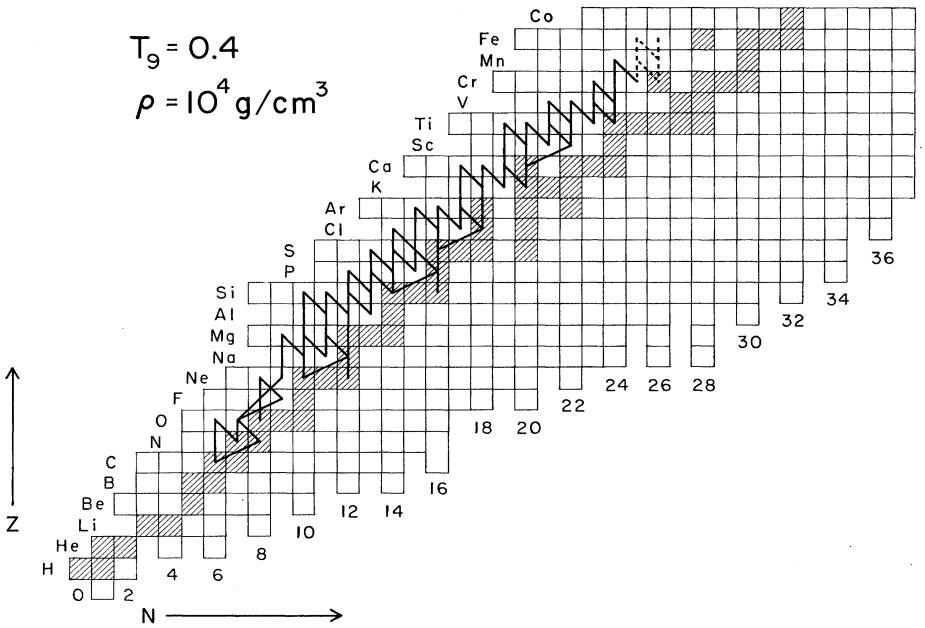

FIG. 1. Sequential and cyclic reaction sequences in hot hydrogen burning. Indicated are the reaction flows integrated over a period of $t=100$ s for a constant temperature of $T=4\times10^8$ K and a density of $\rho=10^4$ g/cm^3. The dashed lines show the additional flow integrated over a period of $t=1000$ s.

range $E_p \geq 0.2$ MeV, but only upper limits have been established for possible lower energy resonances. However, because of the high level density in the excitation range of the respective compound nuclei, the reaction rates are very well approximated by Hauser-Feshbach calculations in the low temperature range [8,9].

The competing ^{31}P$(p,\alpha)^{28}$Si and ^{35}Cl$(p,\alpha)^{32}$S reaction rates are, however, determined by only a few allowed resonances. Because of the typically low Q value for these reactions, α decay is possible only to the $J^\pi=0^+$ ground state. This limits the α channel to natural parity states, with spin and parity determined by the orbital angular momentum l of the α particle, $J=l$ and $\pi=(-1)^l$. The number of (p,α) resonances is therefore considerably smaller than the number of (p,γ) resonances and statistical approximations are not necessarily valid [12,13].

Possible proton unbound natural parity states have been recently identified by both α capture, ^{28}Si$(\alpha,\gamma)^{32}$S and ^{32}S$(\alpha,\gamma)^{36}$Ar, and α transfer, ^{32}S$(^6$Li$,d)^{36}$Ar, reactions. However, direct measurements of ^{31}P$(p,\alpha)^{28}$Si and ^{35}Cl$(p,\alpha)^{32}$S resonances were handicapped by the large beam induced proton background from elastic scattering and background from the ^{11}B$(p,3\alpha)$ reaction [7,9]. For these reasons, only upper limits could be established for possible resonances below $E_p \leq 0.35$ MeV in ^{31}P$(p,\alpha)^{28}$Si [7] and below $E_p \leq 0.87$ MeV in ^{35}Cl$(p,\alpha)^{32}$S [9]. This causes a considerable uncertainty in the ^{31}P(p,α) and the ^{35}Cl(p,α) reaction rates in low temperature regimes where the strengths of these reactions determine the closure of the SiP and the SCl cycles, respectively.

Figure 2 shows the known states in ^{32}S above the proton threshold. Indicated are the levels which have been observed in resonant proton and α capture. Of particular interest are the $(1,2)^-$ state at 9.059 MeV, which has been observed only in ^{31}P$(p,\gamma)^{32}$S [8], and the 3^- state at 9.023 MeV, observed in ^{31}P$(^3$He$,d)^{32}$S [14] and in ^{28}Si$(\alpha,\gamma)^{32}$S [15]. Both levels might contribute strongly to the ^{31}P$(p,\alpha)^{28}$Si reaction.

Figure 3 shows the level diagram of ^{36}Ar above the proton threshold. Marked are the levels observed in resonant proton and α capture. Of considerable importance to the understanding of the reaction rate of ^{35}Cl$(p,\gamma)^{36}$Ar and ^{35}Cl$(p,\alpha)^{32}$S are the two low energy levels at 8.672 MeV and at 8.556 MeV (2^+), respectively, which have not been observed in resonant capture. For ^{35}Cl$(p,\alpha)^{32}$S, the 2^+ state at 8.909 MeV, which has been observed in ^{35}Cl(p,γ) might also contribute considerably to the reaction rate at low temperatures.

Since direct measurements of the low-energy (p,α) and (p,γ) resonances have been proven to be extremely difficult [7,9], we have populated the low energy proton unbound states in ^{32}S and ^{36}Ar by proton transfer reactions, and the particle and gamma decays of these states were measured to determine relative partial widths Γ_γ/Γ, Γ_α/Γ, and Γ_p/Γ. This leads to an improvement in information on these possibly important resonance levels in both the (p,γ) and (p,α) reaction channels.

In the following section the experimental setup is described and the results are discussed. In the last section the astrophysical implications of the measurements are presented.

II. EXPERIMENTAL SETUP AND RESULTS

The proton unbound states in ^{32}S and ^{36}Ar were populated using the ^{31}P$(^3$He$,d)^{32}$S and the ^{35}Cl$(^3$He$,d)^{36}$Ar single particle transfer reactions. Previous investigations of these reactions have demonstrated that many levels in the excitation energy range of interest are strongly populated

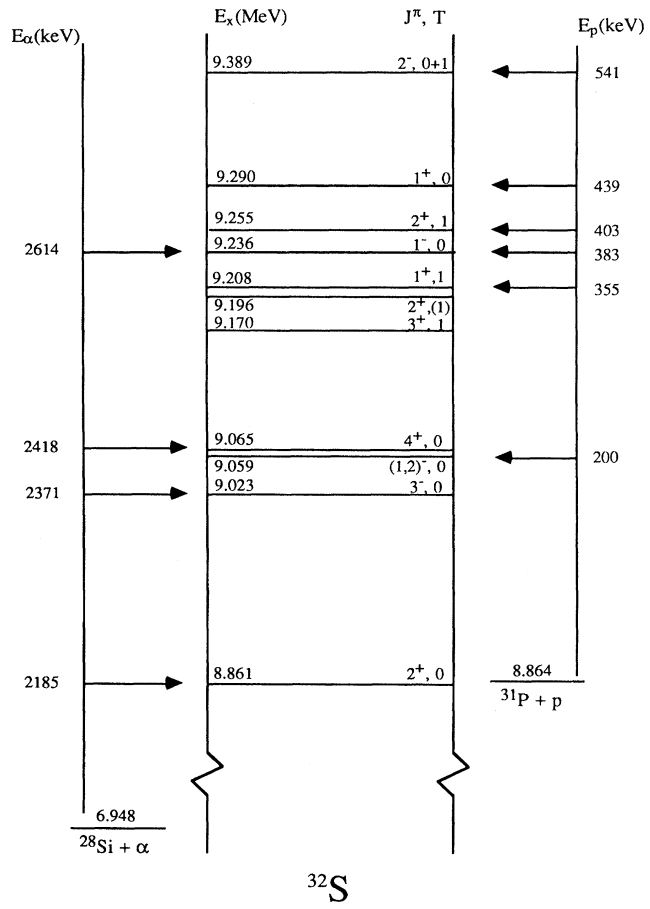

FIG. 2. Level diagram of the proton unbound states in ^{32}S. Indicated are the corresponding center of mass energies of observed resonances in ^{31}P+p and ^{28}Si+α.

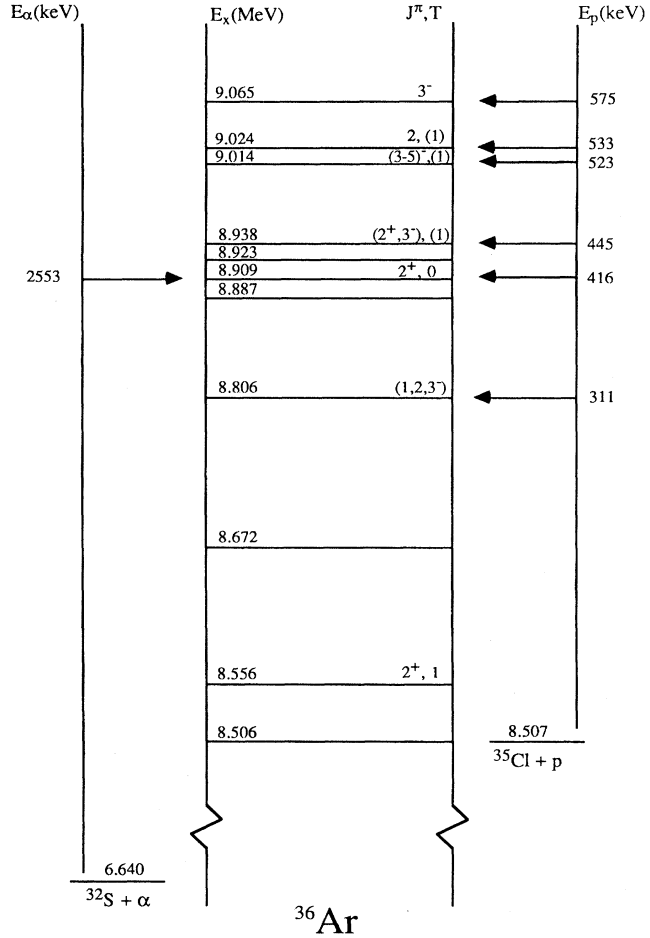

FIG. 3. Level diagram of the proton unbound states in ^{36}Ar. Indicated are the corresponding center of mass energies of observed resonances in ^{35}Cl+p and ^{32}S+α.

[14,9]. This suggests that most of these levels have a pronounced single particle configuration and will also be strongly populated in resonant proton capture.

Both reactions were studied at a ^{3}He beam energy of 25 MeV with an average beam intensity of 50 nA provided by the Princeton AVF cyclotron. Preparation of ^{31}P targets for the ^{31}P(^{3}He,d)^{32}S measurements involved the vacuum evaporation of a Co_2P layer of 30–50 μg/cm^2 thickness on a 40 μg/cm^2 carbon foil; for background measurements an elemental Co target was prepared using similar techniques. For the investigation of ^{35}Cl(^{3}He,d)^{36}Ar an isotopically pure ^{35}Cl target was necessary. The target was prepared by ion implantation into a 40 μg/cm^2 carbon foil using a 60 keV ^{35}Cl beam provided by the Notre Dame SNICS ion source. The implantation resulted in a ^{35}Cl target thickness of 6 μg/cm^2.

The reaction deuterons were detected at $\theta_{\rm lab}=0°$ in the focal plane of the Princeton QDDD magnetic spectrometer (for details see [10]). The typical energy resolution was $\approx$20 keV, sufficient to resolve most of the levels of interest. The energy calibration of the focal plane was performed using well-known strongly populated excited levels in ^{32}S.

Protons and α particles from the decay of the populated states were collected in coincidence with the corresponding deuteron groups using three 450 mm^2 Si surface barrier detectors positioned at back angles $\theta_{\rm lab}$ = 90°, 110°, and 145° with respect to the beam direction at a distance of 9.5 cm to the target. The detectors were energy calibrated with a ^{241}Am α source (E_α=5.48 MeV); their energy resolution was determined to be $\delta E\approx$100 keV. The solid angles of the detectors have been calculated from the geometry of the setup and were measured independently using the strong ^{19}F(^{3}He,$d-\alpha$) reaction to the 0^+ state at 6.725 MeV in ^{20}Ne, which decays 100% into the isotropic $^{16}O_{\rm g.s.}+\alpha$ channel. The use of three detectors allowed a direct measurement of the angular distribution $W(\theta_{p,\alpha})$ of the emitted protons and α particles, which were fitted in terms of Legendre polynomials $P_2(\theta)$ and $P_4(\theta)$,

$$W(\theta_{p,\alpha})=a_0+a_2P_2(\theta)+a_4P_4(\theta) \qquad (2)$$

with $a_0=1/4\pi$.

To measure the γ decay of the populated states, a 12.7×10.2 cm^2 NaI detector was placed in close proximity (5.4 cm) to the target at $\approx$90° to the beam direction. The γ spectra were measured in coincidence with the various deuteron groups. A 3 mm thin lead plate was positioned between detector and target to reduce the count rate of low energy γ rays from the target.

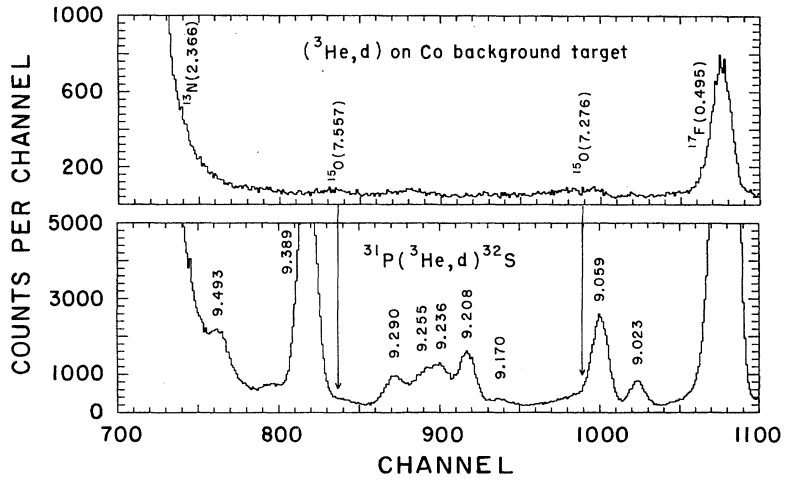

FIG. 4. ^{31}P(^{3}He,d) spectrum of proton unbound states in ^{32}S measured at $\theta_{lab}=0°$ using a Co_2P target. The upper part of the figure shows a background spectrum taken on a Co target under identical conditions.

The intrinsic efficiency $\eta_{int}(E_\gamma)$ of a NaI detector is well understood [17] and was calculated including the geometry of the setup. The γ attenuation ϵ_{attn} in the Al and Pb shielding between target and detector was taken into account. The attenuation coefficients for lead and aluminum $\lambda_{Pb}(E_\gamma)$, $\lambda_{Al}(E_\gamma)$ were taken from standard tabulations [17]. The resulting total efficiency $\eta_\gamma(E_\gamma)=\eta_{int}(E_\gamma)\epsilon_{attn}\approx\eta_\gamma$ is practically independent of the γ energy over the energy range of interest, 1.0 MeV$\leq E_\gamma \leq$9.5 MeV, $\eta_\gamma(E_\gamma)\approx 0.071$. The calculated efficiencies were in good agreement with experimental values obtained from a ^{137}Cs source and the analysis of the γ decay of the well known state at 9.059 MeV in ^{32}S [7].

A. Measurement of ^{31}P(^{3}He,$d-p,\alpha,\gamma$)

Figure 4 shows the spectrum for the ^{31}P(^{3}He,d)^{32}S reaction measured at $\theta_{lab}=0°$. Most of the previously known proton unbound states can be identified. The two levels close to the proton threshold at 9.059 and 9.023 MeV, which have not been observed in resonant proton capture measurements, are well separated. It should be noted that the 4^+ state at 9.065 MeV, which was only identified in ^{28}Si(α,γ) resonant capture, was not observed [8,19]. Shown for comparison is a spectrum taken at the same beam energy with the Co background target. No major contaminants were identified in the momentum range of interest.

The corresponding particle decay spectra (with random events removed) are shown in Fig. 5. The states at 9.208, 9.236, 9.255, and 9.290 MeV in ^{32}S overlap in the deuteron spectrum (see Fig. 4); the deuteron gates were therefore drawn on different areas of each peak in order to extract the number of coincident particles belonging to each state. Proton decay is observed for the higher excited states at 9.255 and 9.389 MeV. Decay into the α channel is observed for the 3^- level at 9.023 MeV and for the 1^- state at 9.236 MeV. No coincident events could be observed for the particle decay of all other levels populated in ^{31}P(^{3}He,d)^{32}S.

The relative partial widths are directly proportional to the number of coincident events $N_{coinc}(d-p,\alpha)$, via

$$\frac{\Gamma_{p,\alpha}}{\Gamma_{tot}}=\frac{N_{coinc}(d-p,\alpha)}{N(d)}[\Omega_{p,\alpha}W(\theta_{p,\alpha})]^{-1}, \quad (3)$$

where $N(d)$ is the number of detected deuterons populating the level, $W(\theta_{p,\alpha})$ is the angular correlation, obtained by fitting the measured angular distribution in the three detectors, and $\Omega_{p,\alpha}$ is the solid angle of the Si-detectors, which is directly determined from coincidence measurements of ^{19}F(^{3}He,$d-\alpha$)^{20}Ne and ^{12}C(^{3}He,$d-p$)^{13}N for states with $\Gamma_{\alpha,p}\approx\Gamma_{tot}$ which decay isotropically.

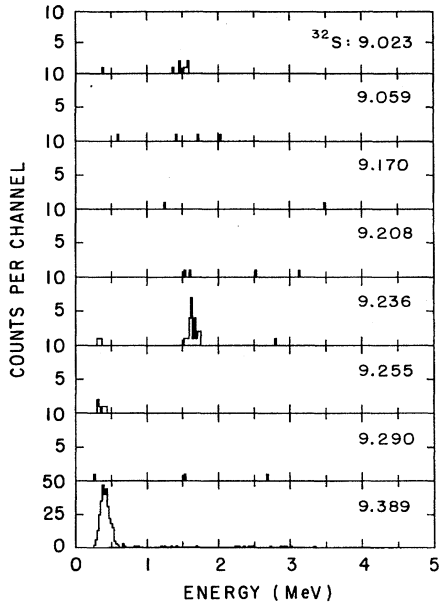

FIG. 5. Particle spectra taken in coincidence with deuterons populating proton unbound states in ^{31}P(^{3}He,d)^{32}S. The details of the proton and α decay of the populated states are discussed in the text.

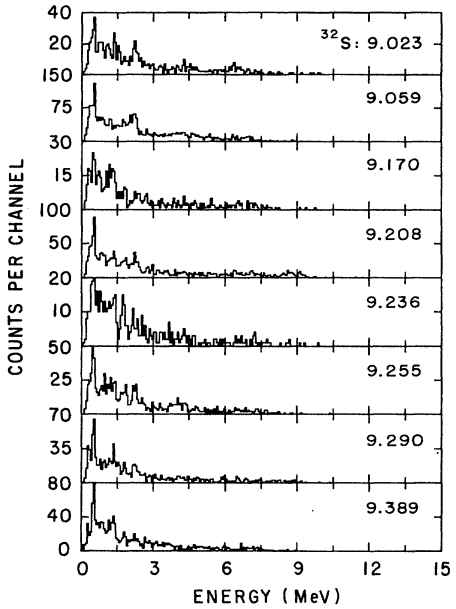

FIG. 6. Gamma spectra taken in coincidence with deuterons populating proton unbound states in ^{31}P(^{3}He,d)^{32}S. The details of the γ decay of the populated states are discussed in the text.

Deuteron-γ coincidences were measured to verify independently the observed small relative particle widths. Figure 6 shows the γ spectra obtained with the NaI detector in coincidence with the deuteron groups populating the proton unbound states in ^{32}S. Due to the limited resolution of the NaI detector and the small number of γ events distributed over the whole spectrum, no new γ branchings for the γ decay of the populated states were obtained. In the spectrum of the 1^+ state at 9.208 MeV a strong ground state transition as well as a transition to the first excited 2^+ state at 2.230 MeV can be clearly identified, in agreement with the results of previous work [7]. The predominant decay of the state at 9.059 MeV to the first excited level at 2.230 MeV also agrees with previous results [8]. The 3^- state at 9.023 MeV, which is of particular interest for the resonant capture, seems to decay preferably to the first excited state at 2.230 MeV (2^+) and to the 2^+ state at 4.282 MeV.

Because of the uncertainties in the γ decay branchings and the low statistics in a given gamma peak, the relative γ partial width was derived from the total number of coincident events in the spectrum, $N_{\text{coinc}}(d-\gamma)$, normalized to the average number of emitted γ's per decay $\langle n_\gamma \rangle$ (see Table I), which was calculated from known γ cascades [7,8]. In the case of the 3^+ state at 9.170 MeV the mean value for the average γ/decay has been adopted. This results in

$$\frac{\Gamma_\gamma}{\Gamma_{\text{tot}}} = \frac{N_{\text{coinc}}(d-\gamma)}{N(d)} [\eta_\gamma \langle n_\gamma \rangle]^{-1}. \quad (4)$$

Because of the large acceptance angle of the detector the γ spectrum is measured over a wide angular range, with an angular correlation $W(\theta\gamma) \approx 1$. The total γ efficiency η_γ is essentially energy independent and has been determined as discussed above.

TABLE I. Relative α and γ widths of proton unbound states in ^{32}S.

E_x (MeV)	E_p^{cm} (MeV)	$J^\pi;T$	$\frac{\Gamma_\alpha}{\Gamma}$	$\langle n_\gamma \rangle$	$\frac{\Gamma_\gamma}{\Gamma}$
9.023	0.159	$3^-;0$	0.37 ± 0.13	2.2	0.75 ± 0.19
9.059	0.194	$(1,2)^-$	≤ 0.03	2.0	1.0 ± 0.2
9.170	0.305	$3^+;1$	≤ 0.08	2.6	1.0 ± 0.3
9.208	0.344	$1^+;1$	≤ 0.05	1.8	1.2 ± 0.3
9.236	0.371	$1^-;0$	1.00 ± 0.08	2.6	≤ 0.15
9.255	0.390	$2^+;1$	≤ 0.08	2.6	0.84 ± 0.22
9.290	0.425	1^+	≤ 0.13	2.0	1.03 ± 0.26
9.389	0.524	2^-	≤ 0.02 [a]	2.2	≤ 0.05

[a] $\Gamma_p/\Gamma = 0.97\pm0.06$.

Table I lists the relative partial widths for all the observed states above the proton threshold. For the levels where no particle decays have been observed, upper limits have been obtained for the relative particle partial widths from the upper limit on the number of coincident events, $\sqrt{2N_{\text{coinc}}(d-p,\alpha)}$ in the spectra. The results indicate that except for the two states at 9.236 MeV and 9.389 MeV the γ decay dominates the other decay channels. The main decay branch of the 1^- level at 9.236 MeV is the α channel, while for the 2^- state at 9.389 MeV the proton width dominates. This confirms the results of previous proton capture studies [7]. For the 3^- low-energy state at 9.023 MeV a fairly strong α branching is observed, but it is only comparable in strength to its γ width. Only upper limits were obtained for the alpha widths of all other proton unbound states.

B. Measurement of ^{35}Cl(^{3}He,$d-p,\alpha,\gamma$)

Figure 7 shows the spectrum of ^{35}Cl(^{3}He,d)^{36}Ar measured at $\theta_{\text{lab}}=0°$. The comparison with the (^{3}He,d) background spectrum from a Melamine target ($C_3H_6N_6$) indicates that some of the observed deuteron groups originate from ^{14}N(^{3}He,d)^{15}O and from ^{16}O(^{3}He,d)^{17}F. The deuteron groups of interest are reasonably well resolved from these contaminant deuterons except for the transition to the state at 9.014 MeV which is unresolved from the ^{14}N(^{3}He,d) transition to the state at 7.557 MeV in ^{15}O. Since the transition to the state at 7.276 MeV in ^{15}O is fairly isolated, the intensity ratio has been used to subtract the background events to determine the counts for the transition to the 9.014 MeV state in ^{36}Ar. All known levels in ^{36}Ar [16] are well resolved except for the doublet at 8.923 and 8.938 MeV. The two natural parity states near the proton threshold at 8.556 MeV (2^+) and at 8.672 MeV [9] are sufficiently strongly populated in the ^{35}Cl(^{3}He,d) reaction to measure particle coincidences.

The particle decay spectra of the populated proton unbound states in ^{36}Ar are shown in Fig. 8. Only the proton decay of the 3^- level at 9.065 MeV has been observed. There is no indication of the α decay of any of the populated levels. Upper limits for the relative α partial widths have been determined from the number of counts in the respective energy range as described above.

These results indicate that all important low-energy proton unbound states in ^{36}Ar decay predominantly into the γ

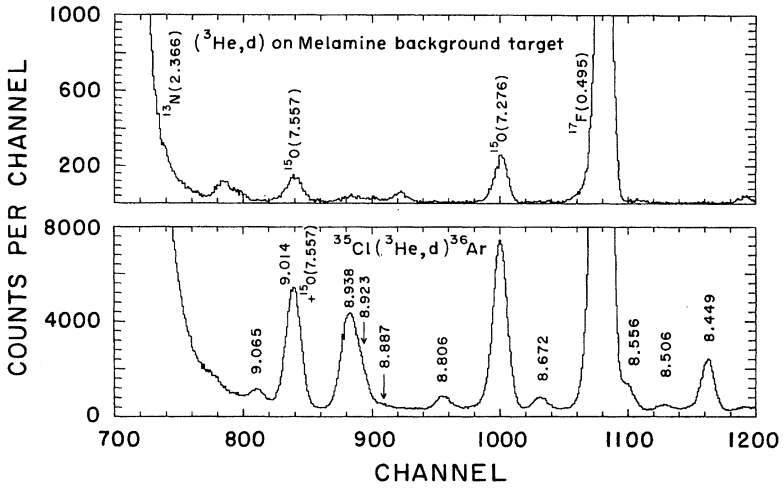

FIG. 7. ^{35}Cl(^{3}He,d) spectrum of proton unbound states in ^{36}Ar measured at $\theta_{lab}=0°$ on an implanted ^{35}Cl target. The upper part of the figure shows a background spectrum taken on a melamine target under identical conditions.

channel. To confirm this, deuteron-γ coincidence measurements were performed in a manner similar to those for ^{32}S discussed in the preceding section. The deuteron gated γ spectra for the individual states are shown in Fig. 9. The γ-decay branchings are well known for the levels above $E_x \geq 8.806$ MeV [9]. This allows a direct calculation of the average number of γ events per decay which are listed in Table II. The γ spectra for the decay of the 2^+ level at 8.556 MeV is dominated by the two transitions to the first excited state at 1.970 MeV ($J^\pi=2^+$) and to the 3^- state at 4.178 MeV. The level at 8.672 MeV decays predominantly to the ground state with a weaker branch to the first excited state. This allows an estimate of the average number of γ's per decay for these two states as well. The total efficiency has been independently confirmed by measuring the known relative partial width of the 7.276 MeV state in ^{15}O, $\Gamma_\gamma/\Gamma_{tot} \approx 1$.

Table II lists the relative partial widths for all the observed states in ^{36}Ar above the proton threshold. Except for the state at 9.065 MeV, the γ decay dominates the other decay channels; the main decay branch of the 3^- level at 9.065 MeV is the proton channel. For the state at 9.014 MeV the relative γ width appears to be too high: this may be explained by the fact that the corresponding deuteron group is contaminated by deuterons from the population of the

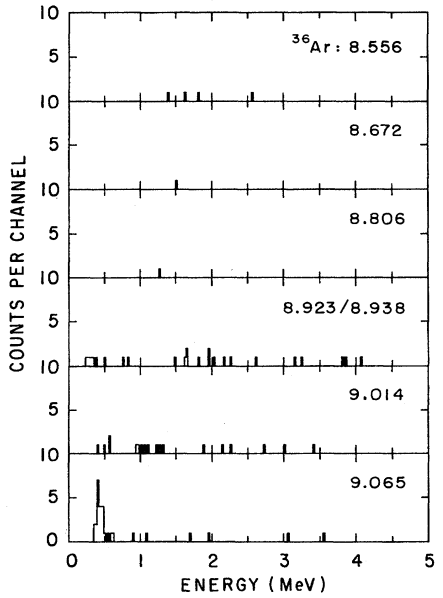

FIG. 8. Particle spectra taken in coincidence with deuterons populating proton unbound states in ^{35}Cl(^{3}He,d)^{36}Ar. The details of the proton and α decay of the populated states are discussed in the text.

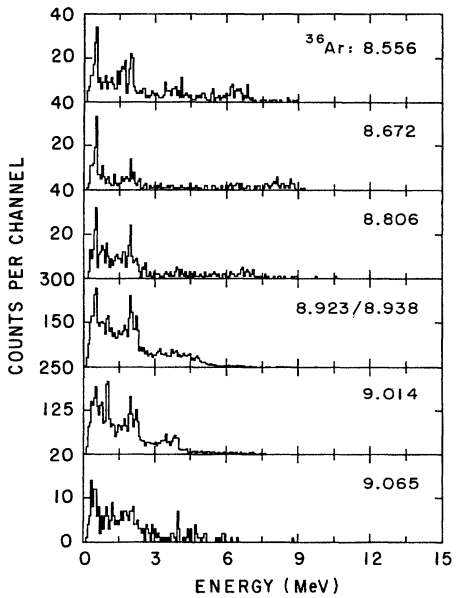

FIG. 9. Gamma spectra taken in coincidence with deuterons populating proton unbound states in ^{35}Cl(^{3}He,d)^{36}Ar. The details of the γ decay of the populated states are discussed in the text.

TABLE II. Relative α and γ widths of proton unbound states in ^{36}Ar.

E_x (MeV)	E_p^{cm} (MeV)	$J^\pi;T$	$\frac{\Gamma_\alpha}{\Gamma}$	$\langle n_\gamma \rangle$	$\frac{\Gamma_\gamma}{\Gamma}$
8.556	0.049	$2^+;1$	≤ 0.07	2.0	1.04 ± 0.25
8.672	0.165		≤ 0.12	1.7	0.8 ± 0.4
8.806	0.302	$(1,2,3)^-$	≤ 0.08	2.0	1.08 ± 0.26
8.887	0.380		≤ 0.2	2.6	1.0 ± 0.3
8.923	0.416		≤ 0.06	2.7	1.0 ± 0.3
8.938	0.433	$2^+,3^-;(1)$	≤ 0.02	3.0	0.94 ± 0.25
9.014	0.508	$(3^- - 5^-);1$	≤ 0.03	3.7	1.47 ± 0.53
9.065	0.559	3^-	≤ 0.14[a]	2.9	0.17 ± 0.05

[a] $\Gamma_p/\Gamma = 0.92 \pm 0.11$.

7.557 MeV state in ^{15}O as discussed above. These current measurements confirm the results of the previous low energy ^{35}Cl$(p,\alpha)^{32}$S studies [9] which showed no indication of strong resonances in the reaction yield. The present experiments demonstrate that for all low energy proton unbound states in ^{36}Ar the α partial width is at least one order of magnitude smaller than the γ partial width.

III. REACTION RATES AND ASTROPHYSICAL IMPLICATIONS

The reaction rates $N_A\langle\sigma v\rangle$ of ^{31}P$(p,\alpha)^{28}$Si, ^{31}P$(p,\gamma)^{32}$S, ^{35}Cl$(p,\alpha)^{32}$S, and ^{35}Cl$(p,\gamma)^{36}$Ar are dominated by the resonant contributions. The reaction rate in units of cm^3 s^{-1} mole^{-1} is expressed as a function of temperature T_9 (in units GK) by

$$N_A\langle\sigma v\rangle = 1.54\times 10^{11}(\mu T_9)^{-3/2}\omega\gamma \exp\left[-\frac{11.605E_r^{cm}}{T_9}\right] \quad (5)$$

and depends on the reduced mass μ, the center of mass resonance energy E_r^{cm} and the resonance strength $\omega\gamma$, both in units MeV. The resonance strengths

$$\omega\gamma_{(p,\alpha)} = \frac{2J+1}{(2j_p+1)(2j_T+1)}\Gamma_p\frac{\Gamma_\alpha}{\Gamma} \quad (6)$$

and

$$\omega\gamma_{(p,\gamma)} = \frac{2J+1}{(2j_p+1)(2j_T+1)}\Gamma_p\frac{\Gamma_\gamma}{\Gamma} \quad (7)$$

depend on the proton partial widths Γ_p and the relative α and γ partial widths Γ_α/Γ and Γ_γ/Γ of the proton unbound states in ^{32}S and ^{36}Ar, listed in Tables I and II. The resonance strengths of most of the (p,γ) resonances on ^{31}P and ^{35}Cl have been measured directly in previous work [7–9] and are compiled in Tables III and IV. However, except for the ^{31}P(p,α) resonance at 371 keV, only upper limits have been obtained from the direct measurement of the resonance strengths in the competing (p,α) channels. The present information allows a reduction in the experimental upper limits on the (p,α) strengths using the relation

$$\omega\gamma_{(p,\alpha)} = \omega\gamma_{(p,\gamma)}\frac{\Gamma_\alpha}{\Gamma_\gamma}. \quad (8)$$

These resulting upper limits are listed in Tables III and IV, in addition to the previous results of direct capture measurements [7,8,18].

Of particular interest are the low energy resonance contributions. In the case of ^{31}P$(p,\gamma)^{32}$S and ^{31}P$(p,\alpha)^{28}$Si, the near-threshold state at 9.023 (3^-) can possibly contribute in both reaction channels. Previous ^{28}Si(α,γ) measurements [15] yield a resonance strength of $\omega\gamma_{(\alpha,\gamma)} = 5.2\times 10^{-2}$ eV. The DWBA analysis of single particle transfer reactions ^{31}P$(^3$He$,d)^{32}$S [14] and ^{31}P$(d,n)^{32}$S [20] to this unbound state, using the method described by Vincent and Fortune [21], yields $(2J+1)\Gamma_p = 9.1\times 10^{-11}$ eV (see Table III) with an uncertainty of approximately 40% [9] depending on the choice of the optical model parameters. Using the relative α width of $\Gamma_\alpha/\Gamma = 0.37 \pm 0.13$, this translates into the resonance strengths of $\omega\gamma_{(p,\alpha)} = (8.4 \pm 4.9)\times 10^{-12}$ eV and $\omega\gamma_{(p,\gamma)} = (1.4 \pm 0.8)\times 10^{-11}$ eV in the respective reaction

TABLE III. Resonance energies and resonance strengths in ^{31}P$(p,\gamma)^{32}$S and ^{31}P$(p,\alpha)^{28}$Si.

E_x (MeV)	E_p (MeV)	J^π	$(2J+1)\Gamma_p$ (eV) [a]	$\omega\gamma_{(p,\gamma)}$ (eV)	$\omega\gamma_{(p,\alpha)}$ (eV)
9.023	0.159	3^-	9.1×10^{-11}	$(1.4 \pm 0.8)\times 10^{-11}$	$(8.4 \pm 4.9)\times 10^{-12}$
9.059	0.194	$(1,2)^-$	4.9×10^{-6}	$(4.8 \pm 1.6)\times 10^{-7}$	$\leq 1.9\times 10^{-8}$
9.065	0.201	4^+		$\leq 3.3\times 10^{-9}$	$\leq 3.3\times 10^{-9}$
9.170	0.305	3^+		$\leq 3.7\times 10^{-5}$	
9.196	0.331	2^+		$\leq 6.1\times 10^{-5}$	$\leq 4.2\times 10^{-4}$
9.208	0.344	1^+	2.4×10^{-2}	$(4.2 \pm 0.7)\times 10^{-3}$	
9.236	0.371	1^-	2.0×10^{-2} [b]	$(6.0 \pm 1.2)\times 10^{-5}$	$(2.7 \pm 0.7)\times 10^{-3}$
9.255	0.390	2^+	2.6×10^{-3}	$(4.5 \pm 0.7)\times 10^{-4}$	$\leq 4.2\times 10^{-5}$
9.290	0.425	1^+	2.8×10^{-1}	$(2.5 \pm 0.4)\times 10^{-2}$	
9.389	0.524	2^-	7.75	$(1.2 \pm 0.2)\times 10^{-1}$	
9.464	0.600	2^+		$(1.1 \pm 0.2)\times 10^{-3}$	$(2.5 \pm 0.4)\times 10^{-2}$

[a] Results of a DWBA analysis of single particle transfer reactions [14,20]. A 40% uncertainty is assigned to the quoted proton widths.

[b] A direct computation from the resonance strengths in the proton and α resonance capture yields, $(2J+1)\Gamma_p = 1.1 \pm 0.4\times 10^{-2}$ [8].

TABLE IV. Resonance energies and resonance strengths in $^{35}Cl(p,\gamma)^{36}Ar$ and $^{35}Cl(p,\alpha)^{32}S$.

E_x (MeV)	E_p (MeV)	J^π	$(2J+1)\Gamma_p$ (eV) [a]	$\omega\gamma_{(p,\gamma)}$ (eV)	$\omega\gamma_{(p,\alpha)}$ (eV)
8.556	0.049	2^+	2.3×10^{-23}	$(2.8\pm1.2)\times10^{-24}$	$\leq2.0\times10^{-25}$
8.672	0.165	(1^-)	2.7×10^{-9}	$(3.4\pm1.6)\times10^{-10}$	$\leq4.0\times10^{-11}$
8.806	0.302	$(1,2,3^-)$		$(1.5\pm0.5)\times10^{-5}$	$\leq1.6\times10^{-6}$
8.887	0.380			$\leq3.1\times10^{-5}$	$\leq6.2\times10^{-6}$
8.909	0.404	2^+		$(6.6\pm3.3)\times10^{-5}$	$\leq1.0\times10^{-3}$
8.923	0.416			$\leq1.3\times10^{-4}$	$\leq7.8\times10^{-6}$
8.938	0.433	$2^+,3^-$		$(1.4\pm0.3)\times10^{-2}$	$\leq3.2\times10^{-4}$
9.014	0.508	(3^--5^-)		$(1.2\pm0.3)\times10^{-3}$	$\leq4.5\times10^{-5}$
9.024	0.518	2		$(3.2\pm0.7)\times10^{-2}$	
9.065	0.559	3^-	4.1×10^{-1}	$(3.1\pm0.6)\times10^{-2}$	$\leq7.2\times10^{-3}$
9.117	0.610	1^-	3.6×10^{-1}	$(7.6\pm1.8)\times10^{-4}$	$\leq1.6\times10^{-1}$

[a]Results of a DWBA analysis of single particle transfer reactions. Values are only given for levels with an unambiguous spin and parity assignment. For more details see Ref. [9]. A 40% uncertainty is assigned to the quoted proton widths.

channels. The 1^- level at 9.236 MeV has been observed in all three capture reaction channels, $^{28}Si(\alpha,\gamma)^{32}S$, $^{31}P(p,\gamma)^{32}S$, and $^{31}P(p,\alpha)^{28}Si$, with resonance strengths of $\omega\gamma_{(\alpha,\gamma)}=0.51\pm0.10$ eV, $\omega\gamma_{(p,\gamma)}=(6.0\pm1.2)\times10^{-5}$ eV, and $\omega\gamma_{(p,\alpha)}=(2.7\pm0.7)\times10^{-3}$ eV, respectively [8]. This allows a direct calculation of the value of $(2J+1)\Gamma_p=(1.1\pm0.4)\times10^{-2}$ eV. This result is in good agreement with the value calculated from the measured single particle spectroscopic factor. Although no coincident alphas were detected for the levels at 9.059 and 9.255 MeV, the measured upper limits on the alpha partial widths result in an order of magnitude reduction in the (p,α) strengths of these states from the previous direct measurements [8]. In the case of the natural parity level at 9.255 MeV, $J^\pi=2^+$, the isospin is $T=1$ and the α decay is isospin forbidden, as reflected in the present result.

In the case of $^{35}Cl(p,\gamma)^{36}Ar$ and $^{35}Cl(p,\alpha)^{32}S$ the two levels at 8.556 (2^+) at 8.672 MeV ($\leq4^+$) will possibly contribute in both reaction channels. Only upper limits have been determined in the previous direct measurements [9]. The DWBA analysis of $^{35}Cl(^3He,d)^{36}Ar$ transfer studies [9] provides the proton partial widths $(2J+1)\Gamma_p$ listed in Table IV. The present results (see Table II) indicate that both levels decay predominantly into the γ channel. The resonance strengths in the (p,γ) channel are therefore determined by $\omega\gamma_{(p,\gamma)}=(2J+1)\Gamma_p/8$ following equation (7), and are listed in Table IV. The resonance strength of the 8.672 MeV level depends on the spin assignment for this state which was not uniquely determined from the angular distribution measurements, $J^\pi\leq4^+$. An $l=1$ transfer does however appear the most likely [9,22]. This state is populated in $^{32}S(^6Li,d)^{36}Ar$ α transfer, which suggest a natural parity assignment. Therefore, we suggest a tentative assignment of $J^\pi=1^-$ for this level. The upper limits for the relative α widths have been used to calculate the upper limits for $\omega\gamma_{(p,\alpha)}$ using Eq. (8) and are also listed in Table IV.

The 2^+ state at 8.909 MeV has been observed in $^{35}Cl(p,\gamma)^{36}Ar$ and in $^{32}S(\alpha,\gamma)^{36}Ar$, but was not observed in $^{35}Cl(p,\alpha)^{32}S$ [9]. This level is also not populated in the $^{35}Cl(^3He,d)^{36}Ar$ single particle transfer and therefore the relative partial widths are not determined. The upper limit cross section for an $l=0$ transfer yields an upper limit for the proton width of the state, $(2J+1)\Gamma_p\leq8.5\times10^{-3}$ eV. This and the resonance strengths $\omega\gamma_{(p,\gamma)}$ and $\omega\gamma_{(\alpha,\gamma)}$ give an upper limit for the resonance strength in the (p,α) channel, $\omega\gamma_{(p,\alpha)}\leq1.0\times10^{-3}$ eV.

The reaction rates have been calculated using Eq. (5) and are shown in Figs. 10 and 11 as a function of temperature. Shown are the contributions of all previously observed higher energy resonances as well as the contributions of the presently considered low energy resonances.

The resonance at $E_r^{cm}=159$ keV in $^{31}P(p,\gamma)$ is negligible compared to the contributions of the low energy resonances at $E_r^{cm}=194$ keV and 344 keV [8]. At temperatures $T\geq5\times10^8$ K, the reaction rate is dominated by the contribution of the higher energy resonances at $E_r^{cm}=440$ keV, 524 keV, and 600 keV [7]. In $^{31}P(p,\alpha)$ the resonance at $E_r^{cm}=159$ keV can dominate the reaction rate at temperatures $T\leq10^8$ K if the state at 9.059 MeV does not decay into the α channel. At higher temperatures $T\geq10^8$ K, the reaction rate is entirely

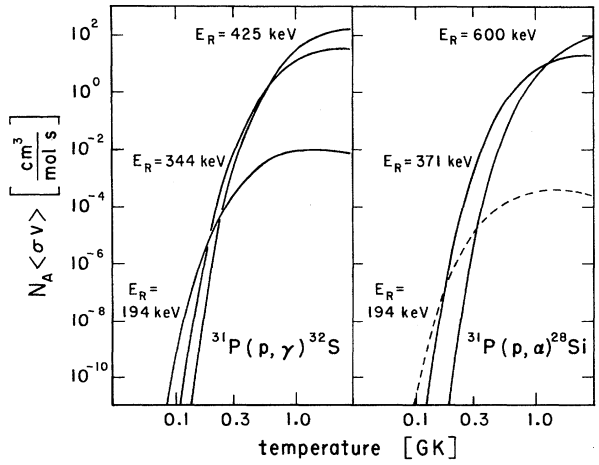

FIG. 10. The reaction rates of $^{31}P(p,\alpha)^{28}Si$ and $^{31}P(p,\gamma)^{32}S$ as a function of temperature. The solid lines indicate the contribution of the experimentally known resonances; the dashed lines indicate the upper limits of low energy resonances not observed in the present experiment.

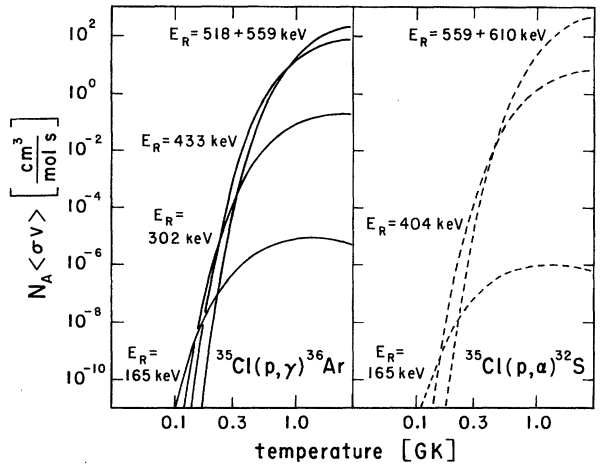

FIG. 11. The reaction rates of $^{35}\mathrm{Cl}(p,\alpha)^{32}\mathrm{S}$ and $^{35}\mathrm{Cl}(p,\gamma)^{36}\mathrm{Ar}$ as a function of temperature. The solid lines indicate the contribution of the experimentally known resonances; the dashed lines indicate the upper limits of low energy resonances not observed in the present experiment.

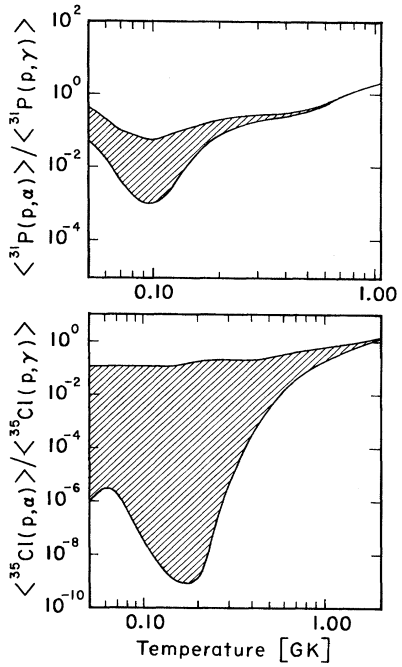

FIG. 12. The ratio of the reaction rates of $^{31}\mathrm{P}(p,\alpha)^{28}\mathrm{Si}$ and $^{31}\mathrm{P}(p,\gamma)^{32}\mathrm{S}$, and of $^{35}\mathrm{Cl}(p,\alpha)^{32}\mathrm{S}$ and $^{35}\mathrm{Cl}(p,\gamma)^{36}\mathrm{Ar}$ as a function of temperature. The dashed areas indicate the range of uncertainty in the $^{31}\mathrm{P}(p,\alpha)^{28}\mathrm{Si}$ and in the $^{35}\mathrm{Cl}(p,\alpha)^{32}\mathrm{S}$ reactions. The upper limit corresponds to the experimental upper limit for the (p,α) strengths for the unbound states in $^{32}\mathrm{S}$ and $^{36}\mathrm{Ar}$; the lower limit neglects all resonance contributions from levels unobserved in the α capture or decay channel.

dominated by the contribution of the previously known resonances at $E_r^{\mathrm{cm}}=371$ keV and 600 keV [7].

Figure 12 shows the ratio of the $^{31}\mathrm{P}(p,\alpha)$ and $^{31}\mathrm{P}(p,\gamma)$ reaction rates as a function of temperature. The dashed area indicates the range of experimental uncertainty. The upper curve is calculated including the upper limits of the unobserved resonances in $^{31}\mathrm{P}(p,\alpha)$, while the lower curve is based only on the resonance contributions of observed levels. The results suggest that the $^{31}\mathrm{P}(p,\gamma)$ reaction is up to two orders of magnitude stronger than the competing $^{31}\mathrm{P}(p,\alpha)$ rate. This confirms the previous results that at low temperatures, even with possible contributions from the 159 keV resonance, break out from the SiP cycle dominates the reaction flow, and at most a weak cycle emerges in this mass range (see also [23]).

The reaction rate of $^{35}\mathrm{Cl}(p,\gamma)$ has been discussed before [9]. Figure 11 shows that the low-energy resonance at $E_r^{\mathrm{cm}}=165$ keV influences the rate only at temperatures $T\leq 2\times 10^8$ K. At higher temperatures the reaction rate is dominated by the contributions of the higher-energy resonances at $E_r^{\mathrm{cm}}=302$ keV, 404 keV, 559 keV, and 610 keV. The rate for $^{35}\mathrm{Cl}(p,\alpha)$ is determined by the contribution of the possible resonance at $E_r^{\mathrm{cm}}=165$ keV for temperatures $T\leq 1.5\times 10^8$ K. At higher temperatures the reaction rate is dominated by the contribution of the two natural parity resonances at $E_r^{\mathrm{cm}}=404$ keV (2^+) and 610 keV (1^-). These contributions, however, are only upper limits since no α decay of the corresponding levels was observed in the present work. For temperatures $T\geq 10^9$ K the reaction rate is determined by the contributions of previously observed resonances [24].

Figure 12 shows also the ratio of the $^{35}\mathrm{Cl}(p,\alpha)$ and $^{35}\mathrm{Cl}(p,\gamma)$ reaction rate as a function of temperature. The dashed area indicates the range of experimental uncertainty. The upper curve is calculated including the upper limits of the unobserved resonances in $^{35}\mathrm{Cl}(p,\alpha)$ listed in Table IV, while the lower curve includes only the contributions of previously observed resonances at higher energies [24]. Also included are the tail contributions of observed high-energy resonances below 1.2 MeV. The results suggest that in the entire temperature range below 10^9 K the $^{35}\mathrm{Cl}(p,\gamma)$ break out reaction from the SCl cycle dominates the flow. Therefore only weak cycling characterizes the reaction flow in this mass range. The combination of these results indicates that in hot hydrogen burning less than ten percent of the processed S,Cl material remains stored in the SCl cycle, while the bulk of the material is being processed towards Ca.

IV. CONCLUSION

A direct measurement of low-energy resonances in proton capture reactions like $^{31}\mathrm{P}(p,\gamma)^{32}\mathrm{S}$, $^{31}\mathrm{P}(p,\alpha)^{28}\mathrm{Si}$ and $^{35}\mathrm{Cl}(p,\gamma)^{36}\mathrm{Ar}$, $^{35}\mathrm{Cl}(p,\alpha)^{32}\mathrm{S}$ is difficult because of the high Coulomb barriers for low-energy protons and α particles. Indirect methods, such as discussed here, can give important additional information about the level structure of the compound nucleus. This allows a reliable estimate of the reaction rates usually sufficient for nucleosynthesis network calculations.

Based on these rates it can be concluded that the $^{31}\mathrm{P}(p,\alpha)^{28}\mathrm{Si}$ reaction is weaker by at least one order of magnitude than the competing $^{31}\mathrm{P}(p,\gamma)^{32}\mathrm{S}$ reaction. This reduces the influence of cyclic processing in the Si,P mass range considerably. Also in the case of proton capture on $^{35}\mathrm{Cl}$ the weak $^{35}\mathrm{Cl}(p,\alpha)^{32}\mathrm{S}$ reaction reduces the influence

of cyclic hydrogen burning in the S,Cl range. Therefore, based on the present measurements and the previous results for $^{27}Al(p,\alpha)^{24}Mg$ [6,10], no reaction cycles are expected beyond the NeNa cycle under conditions of hot hydrogen burning, and the reaction path above mass $A=24$ will be characterized by a continuous sequence of proton capture reactions and β decays.

ACKNOWLEDGMENTS

The authors would like to thank Amir Razzaghi for the technical support during the experiment. This project was supported by the NSF Grant Nos. PHY88-03035 (Notre Dame) and PHY93-12588 (Princeton) and the DOE Grant No. DE-FG02-91ER40609 (Yale).

[1] R.K. Wallace and S.E. Woosley, Astrophys. J. Suppl. **45**, 389 (1981).

[2] L. Van Wormer, J. Görres, C. Iliadis, M. Wiescher, and F.K. Thielemann, Astrophys. J. **432**, 326 (1994).

[3] M. Politano, S. Starrfield, J.W. Truran, A. Weiss, and W.M. Sparks, Astrophys. J. (submitted); S. Starrfield, J.W. Truran, M. Politano, W.M. Sparks, I. Nofar, and G. Shaviv, Phys. Rep. **227**, 223 (1993).

[4] A. Coc, R. Mochkovitch, Y. Oberto, J.P. Thibaud, and E. Vangioni-Flam, Astron. Astrophys. (in press).

[5] J. Görres, M. Wiescher, and C. Rolfs, Astrophys. J. **343**, 356 (1989).

[6] R. Timmermann, H.W. Becker, C. Rolfs, U. Schröder, and H.P. Trautvetter, Nucl. Phys. **A477**, 105 (1988).

[7] C. Iliadis, U. Giesen, J. Görres, S.M. Graff, M. Wiescher, R.E. Azuma, J. King, M. Buckby, C.A. Barnes, and T.R. Wang, Nucl. Phys. **A533**, 153 (1991).

[8] C. Iliadis, J. Görres, J.G. Ross, K.W. Scheller, M. Wiescher, C. Grama, Th. Schange, H.P. Trautvetter, and H.C. Evans, Nucl. Phys. **A559**, 83 (1993).

[9] C. Iliadis, J. Görres, J.G. Ross, K.W. Scheller, M. Wiescher, R.E. Azuma, G. Roters, H.P. Trautvetter, and H.C. Evans, Nucl. Phys. **A571,** 132 (1994).

[10] A.E. Champagne, C.H. Cella, R.T. Kouzes, M.M. Lowry, P.V. Magnus, M.S. Smith, and Z.Q. Mao, Nucl. Phys. **A487,** 433 (1988).

[11] G. Hardie, R.E. Segel, A.J. Elwyn, and J.E. Monahan, Phys. Rev. C **38**, 2003 (1988).

[12] S.E. Woosley, W.A. Fowler, J.A. Holmes, and B.A. Zimmerman, Atomic Data Nucl. Data Tables **22**, 371 (1978).

[13] J.J. Cowan, F.K. Thielemann, and J.W. Truran, Phys. Rep. **208**, 268 (1991).

[14] J. Kalifa, J. Vernotte, Y. Deschamps, F. Pougheon, G. Rotbard, M. Vergnes, and B.H. Wildenthal, Phys. Rev. C **17**, 1961 (1978).

[15] W.O. Rogers, W.R. Dixon, and R.S. Storey, Nucl. Phys. **A281**, 345 (1977).

[16] P.M. Endt, Nucl. Phys. **A521**, 1 (1990).

[17] J.B. Marion and F.C. Young, *Nuclear Reaction Analysis Graphs and Tables* (North-Holland, Amsterdam, 1968).

[18] B.M. Paine and D.G. Sargood, Nucl. Phys. **A331**, 389 (1979).

[19] J.D. MacArthur, S.P. Kwan, H.B. Mak, W.D. Latchie, S.A. Page, S.S. Wang, and T.K. Alexander, Phys. Rev. C **32**, 314 (1985).

[20] K. Miura, T. Tohhei, T. Nakagawa, A. Satoh, T. Ishimatsu, T. Kawamura, K. Furukawa, M. Kabasawa, Y. Takahashi, H. Orihara, T. Niizeki, K. Ishii, and H. Ohnuma, Nucl. Phys. **A467**, 79 (1987).

[21] C.M. Vincent and H.T. Fortune, Phys. Rev. C **2**, 782 (1970).

[22] M.A. Moinester and W. Parker Alford, Nucl. Phys. **A145**, 143 (1970).

[23] S. Vouzoukas, C.P. Browne, U. Giesen, J. Görres, S.M. Graff, H. Herndl, C. Iliadis, L.O. Lamm, J. Meissner, J.G. Ross, K. Scheller, L. Van Wormer, M. Wiescher, and A.A. Rollefson, Phys. Rev. C **50**, 1185 (1994).

[24] B. Bosnjakovic, J. Bouwmeester, J.A. van Best, and H.S. Pruys, Nucl. Phys. **A110**, 17 (1968).